SLAC-PUB--4618
DE88 012731

SLAC - PUB - 4618
May 1988
(A)

THE CALCULATED LONGITUDINAL IMPEDANCE OF THE SLC DAMPING RINGS*

KARL L. F. BANE
Stanford Linear Accelerator Center, Stanford University, Stanford, California 94309

Introduction

A high level of current dependent bunch lengthening has been observed in the north damping ring of the Stanford Linear Collider (SLC),[1] indicating that the ring's impedance is very inductive. This level of bunch lengthening will limit the performance of the SLC. In order to study the problem of bunch lengthening in the damping rings and the possibility of reducing their inductance we compute, in this report, the longitudinal impedance of the damping ring vacuum chamber. More specifically we find the response function of the ring to a short gaussian bunch. This function will later be used as a driving term in the longitudinal equations of motion.[2] We also identify the important inductive elements of the vacuum chamber and estimate their contribution to the total ring inductance. This information will be useful in assessing the effect of vacuum chamber modifications. A more detailed discussion of the calculations will be given in Ref. 3.

Inductive Vacuum Chamber Elements

The SLC damping ring vacuum chamber contains many small discontinuities — such as shallow steps, transitions, masks, and bellows — which are normally inductive. When a bunch passes by an inductive object the slope of the induced voltage — over the bunch core — is of the opposite sign of the slope of the rf wave. Such objects will tend to lengthen the bunch. The ring also contains a few deeper objects — primarily the rf cavities — which are normally capacitive. The slope of the induced voltage of a capacitive device is of the same sign as the slope of the rf wave, and such objects will tend to shorten the bunch. It is important to note that whether an object is inductive or capacitive depends critically on the length of the driving charge. Vacuum chamber objects appear more inductive to longer bunches, more capacitive to shorter bunches.

Most of the inductive elements in the damping ring are almost lossless over the operating bunch lengths and can be represented as pure inductors; *i.e.*, the induced voltage $V_{\rm ind}$ — the wakefield times the charge in the bunch — can be well approximated by the formula

$$V_{\rm ind} = -L\frac{dI}{dt} \quad , \tag{1}$$

with I the bunch current, L a constant called the inductance, and t the time. The validity of Eq. (1) implies that the bunch sees primarily the low frequency part of the object's impedance, where it is purely imaginary, and linear with a slope of $-L$. Note that if an object is a good inductor at a certain bunch length, it will continue to be so at longer bunch lengths.

It is normally easy to see whether or not an object is a good inductor for a gaussian bunch with length σ. For example, suppose we have an obstruction in a tube of radius a. If the bunch length obeys the relation $\sigma \gtrsim a/2$ then little of its power spectrum ($\lesssim 9\%$) is above the tube cutoff frequency. When the beam passes by the obstruction it will therefore leave little energy behind, since the tube will not support free waves below its cutoff. The head of the beam will lose energy to the discontinuity, but the tail will reabsorb most of it, resulting in an inductive wakefield. In the SLC damping rings there are many small discontinuities on tubes of radius 11 mm (or less) which, according to our criterion, are good inductors for bunch lengths down to 5.5 mm.

*Work supported by the Department of Energy, contract DE-AC03-76SF00515.

In this paper, in order to quantify the inductiveness of a vacuum chamber discontinuity, we first compute the wakefield of a gaussian bunch passing by the object using T. Weiland's computer program TBCI.[4] We then perform a least squares fit to Eq. (1) — weighted by the current distribution — to obtain the effective inductance L. If the object is a good inductor the results will change little when the bunch length is increased. For the calculations we only consider objects connected to equal sides tubes, so that the system's potential energy is the same at the beginning as at the end of the calculation.

Some Simple Inductors

When a bunch with $\sigma/a \gtrsim 1/2$ passes by the small cavity of Fig. 1a it induces a voltage across the gap that — according to Faraday's Law — depends on the time rate of change of the magnetic flux φ_m in the cavity. If we approximate φ_m by the product of the beam's unperturbed magnetic field at the cavity times the cavity cross-sectional area, we obtain the inductance of this object[7]

$$L = \varphi_m/I = \frac{Z_0}{2\pi c}\frac{g\Delta}{a} \qquad \Delta/a \text{ small} , \tag{2}$$

with I the beam current and $Z_0 = 377\ \Omega$. The inductance of a bellows — which is a sequence of small cavities — can be approximated by the above result multiplied by the number of convolutions.

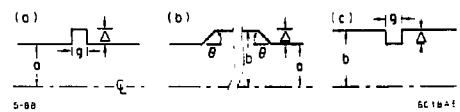

Fig. 1. Some simple vacuum chamber elements: (a) a small cavity, (b) a symmetric pair of shallow transitions, (c) a shallow iris.

We have done parametric studies of a shallow iris (see Fig. 1c) using TBCI, as described earlier, making sure that the bunch is long enough for us to have reached the asymptotic value of L. For small g, we find that the numerical results agree well with

$$L = \frac{Z_0}{\pi c}\frac{\Delta^2}{b} \qquad \Delta/b \text{ small}, \ g/b \text{ small} . \tag{3}$$

From similar studies performed on a pair of symmetric, shallow transitions (Fig. 1b) we find that the inductance — if the transitions are separated by a distance at least on the order of b — can be approximated by

$$L = \frac{3Z_0}{2\pi c}\frac{a\Delta^2}{b^2}\left(\frac{2\theta}{\pi}\right)^{1/2} \qquad \Delta/b \text{ small}, g/b \gtrsim 1, \theta \le \pi/2 . \tag{4}$$

We see that by changing the angle of a transition its inductance can be reduced, although only very slowly. However, if we break up a transition into n smaller steps, which are sufficiently separated, we can gain by the factor n. Equation (4) approximates the numerical results well even for $\Delta/b \sim .5$. Note that the inductance of the iris of Fig. 1c must also be given by Eq. (4) with $\theta = \pi/2$ when $g/b \gtrsim 1$. From the simulations we also find that the losses of these simple inductors decrease exponentially fast as the bunch length is increased. This is understandable since only for the tails of the beam's spectrum — above cutoff — is the real part of the impedance nonzero. More details of our parametric studies will be given in Ref. 3.

Contributed to the European Particle Accelerator Conference, Rome, Italy, June 7–11, 1988

Finally we point out that the inductance formulas of this section may be used to estimate the imaginary part of the transverse impedance $\Im m(Z_\perp)$ at the origin for these structures. Using a well-known formula[5] for estimating the transverse from the longitudinal impedance for a cylindrically symmetric structure, with tube radius a, we find near the origin

$$\Im m(Z_\perp) \approx \frac{2c}{a^2} L \quad . \tag{5}$$

Layout of the Damping Ring Vacuum Chamber

The damping ring vacuum chamber is divided into 8 girders (see Fig. 2). Girders 2, 3, 6 and 7 are almost identical. Each of these girders contains 4 1/2 FODO cells, with the quadrupole vacuum chambers — which are cylindrically symmetric — separated by the roughly rectangular bend vacuum chambers (see Fig. 3). Girders 5 and 8, in addition to half a FODO cell on each end, contain kickers, septa, rf cavities and other vacuum chamber elements not found in the rest of the ring.

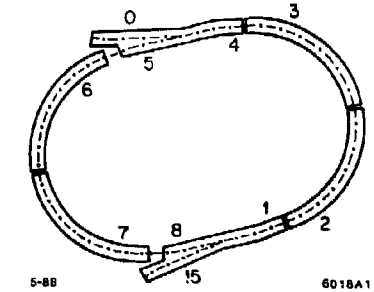

Fig. 2. The girders of the SLC north damping ring.

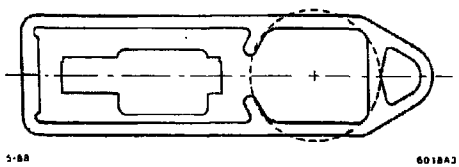

Fig. 3. The cross section of the bend chamber. The dashed circle shows the size of a quad chamber.

The vacuum chamber of the FODO cells can be divided into two groups of objects, each of which is repeated 20 times in the ring. One group, which we will call a "QD vacuum chamber segment" is centered on a defocusing quadrupole vacuum chamber, with each end at the middle of the neighboring bend chamber. The "QF vacuum chamber segment" is similar, though centered on a focusing quadrupole. The vertical profile of these segments is sketched in Fig. 4, with the ends truncated. Nonsymmetric portions are shown dashed. The figures are drawn to scale. The total length of each type is about 60 cm; the half-length of the bend chamber is 15 cm.

A QD segment (see the top sketch) begins with the roughly rectangular bend chamber (1), which is connected by a tapered transition (2) to the cylindrically symmetric defocusing quadrupole (QD) chamber. The QD chamber contains a 1 inch beam position monitor (1" BPM) (3), a QD bellows (4), a serf gasket (5), and a QD mask (6). Finally there is another transition (7) into the next bend (8). The ends of a QF segment are similar (see the bottom of Fig. 4). The cylindrically symmetric QF chamber, however, contains a 1" BPM (3), a flex joint (4), and a QF mask (5).

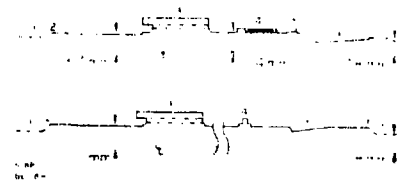

Fig. 4. The vertical profile of a QF segment (top) and a QD segment (bottom). The noncylindrically symmetric portions are drawn with dashes.

Ring girders 5 and 8 include two kickers, two septa, a two cell rf cavity, two 1" to 2" transitions, four 2" BPM's, four 1.4" BPM's, an optical monitor and a dielectric gap.

Inductances of Individual Vacuum Chamber Elements

We have divided the damping ring vacuum chamber into a number of recognizable pieces, for which we have then calculated the effective inductance L (as described earlier), in order to get an estimate of their relative importance for bunch lengthening. Such an approach is reasonable so long as neighboring pieces are not too near each other and so long $\sigma \gtrsim a/2$, with a the tube radius. Whenever possible noncylindrically symmetric objects were modeled by cylindrically symmetric ones that were deemed suitable. Table 1 gives the results for the elements that are inductive to a 6 mm bunch — the nominal bunch length at a ring voltage of .6 MV. The factor in column 3 is an azimuthal filling factor used to account for the contribution of noncylindrically symmetric objects. We see that the QD bellows, the masks, and the bend-to-quad chamber transitions account for roughly 60% of the ring inductance at a bunch length of 6 mm.

Table 1. The inductive vacuum chamber elements.

Single Element Inductance		Contribution in Ring		
Type	L/(nH)	Factor	Number	L/(nH)
QD bellows	.62	1.0	20	12.5
QD & QF masks	.47	1.0	20	9.5
QD & QF trans.	.52	.9	20	9.3
ion pump slots	1.32	.1	40	5.3
kicker bellows	2.03	1.0	2	4.1
flex joint	.18	1.0	20	3.6
1" BPM trans.	.10	.8	40	3.3
other				2.4
		Total		50.0

Not included in the table are the septa, each of which is a complicated obstruction in a 25 mm ID tube, and is therefore inductive. Using the computer program MAFIA[6] on a simple three-dimensional model we estimate that $L \approx 2$ nH for each septum.

There are objects in the ring which are resistive, most important of which are the two 2-cell rf cavities and the forty 1" BPM cavities. At a bunch length of 6 mm the rf cavities contribute 5.8 V/pC to the ring loss factor k; we estimate that the 1" BPM's contribute 3.2 V/pC. Other objects that are resistive at this bunch length, but contribute little to the ring

loss are two 2" BPM's, two 1.4" BPM's, two kicker gaps, an optical monitor, the ion pump holes and a dielectric gap.

The Green Function Computation

For our Green function we have calculated the wakefield of a 1 mm gaussian bunch, out to 15 cm behind the bunch, for the various damping ring vacuum chamber objects. The only exception is for the rf cavities, where a 2.7 mm bunch was used, due to limitations in the computer memory available to us. In order to properly include the interference effects of neighboring objects at frequencies above cutoff, the wakefields of the entire QD and QF segments were each calculated in one piece. To account for the noncylindrical symmetry of the BPM electrodes we have performed the calculation for each segment twice — once with and once without cylindrically symmetric electrodes — and then added the two results in the ratio 8:2, according to the azimuthal filling factor of the real electrodes. However, the calculations of the pump slots, as well as of the remaining objects found in girders 5 and 8, were all done separately. Objects that were not included are the septa, the ion pump holes, the optical monitor, and the dielectric gap. The resulting Green function is shown in Fig. 5.

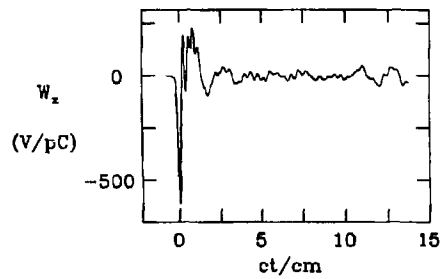

Fig. 5. The longitudinal wakefield of a 1 mm gaussian bunch in the SLC damping ring.

By convolving the Green function with the current distribution of a 6 mm gaussian bunch, we obtain the wakefield shown in Fig. 6, which is clearly very inductive. In Fig. 7 we dispay the ring loss factor k and the effective inductance L due to a gaussian bunch, for a range of bunch lengths. The dotted curve gives the loss contribution of the rf cavities alone. Finally by taking the fast fourier transform of the Green function we obtain the impedance. In Fig. 8 we plot $|Z/n|$ (note that the ring circumference is 35 m). We see a large peak at 16 GHz, with peak value 5.5 Ω, and Q of 2, which is mostly due to the bellows. A smaller resonance, at 6.5 GHz, with peak value 4.4 Ω, and a Q of about 1, is due to the BPM cavities. Our calculation results for this resonance may be very inaccurate, due to the very approximate manner in which we included the BPM electrodes. The constant value of $|Z/n|$ at high frequency is due to numerical noise. Also on the plot — in dots — is the ring impedance with the QD bellows shielded, which, as we see, leads to a substantial reduction in impedance.

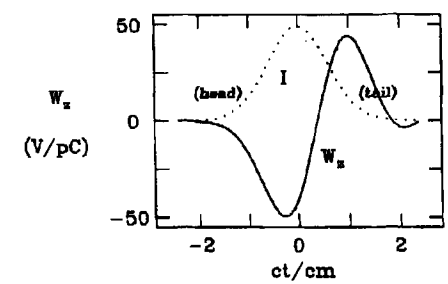

Fig. 6. The longitudinal wakefield of a 6 mm gaussian bunch in the SLC damping ring. The current distribution is also shown.

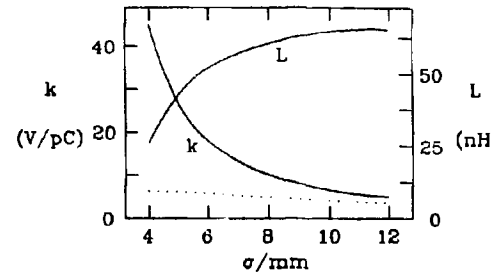

Fig. 7. The loss factor k and the effective inductance L of the damping ring as function of bunch length. The dotted curve gives the loss contribution of the rf.

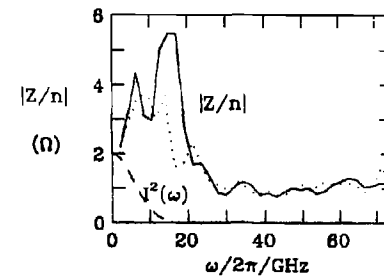

Fig. 8. The impedance $|Z/n|$ of the damping ring. The dots give what remains when the QD bellows (with their antichambers) are perfectly shielded. The power spectrum of a 6 mm gaussian bunch is also shown.

Acknowledgements

The author is grateful to J. Weaver and D. Wright for deciphering blueprints of the damping ring for him. He has also greatly profited from discussions with R. Ruth and T. Weiland on the subject of wakefields and their computation.

References

[1] L. Rivkin *et al.*, "Bunch Lengthening in the SLC Damping Rings," these procedings.

[2] K. Bane and R. Ruth, "Bunch Lengthening in Electron Storage Rings," these proceedings.

[3] K. Bane, "The Impedance of the SLC Damping Rings," SLAC/AP 70, to be published.

[4] T. Weiland, DESY 82-015 (1982) and *Nucl. Inst. Meth.* **212**, 13 (1983).

[5] F. Sacherer, CERN Report 77-13, 198 (1977).

[6] R. Klatt and T. Weiland, 1986 Linear Accelerator Conference Proceedings, SLAC, p. 282.

[7] E. Keil and B. Zotter, *Particle Accelerators* **3**, 11 (1972).

DISCLAIMER